104 MeV Alpha Particle and 156 MeV ^{6}Li Scattering and the Validity of Refined Folding Model Approaches for Light Complex Projectile Scattering

Z. Majka, H. J. Gils, H. Rebel
Institut für Angewandte Kernphysik

Kernforschungszentrum Karlsruhe

KERNFORSCHUNGSZENTRUM KARLSRUHE

Institut für Angewandte Kernphysik

KfK 2622

104 MeV ALPHA PARTICLE AND 156 MeV ^{6}Li SCATTERING AND
THE VALIDITY OF REFINED FOLDING MODEL APPROACHES FOR
LIGHT COMPLEX PROJECTILE SCATTERING

Z. Majka[+], H.J. Gils and H. Rebel

[+] On leave from Institute of Physics, Jagellonian
University, Cracow, Poland

Zusammenfassung

104 MEV ALPHA-TEILCHEN- UND 156 MEV ^{6}LI-STREUUNG IM LICHTE VER-
FEINERTER FALTUNGSMODELLE FÜR DIE STREUUNG LEICHTER KOMPLEXER
PROJEKTILE

Der Realteil des Optischen Potentials für elastische 104 MeV
α-Teilchen-Streuung und 156 MeV ^{6}Li-Streuung an ^{40,48}Ca wurde
auf der Basis halbmikroskopischer Faltungsmodelle berechnet.
Die Gültigkeit und Zuverlässigkeit verschiedener Näherungen
wurde durch Vergleich der Modellvorhersagen mit experimentellen
Wirkungsquerschnitten untersucht, die mit hoher Winkelgenauig-
keit gemessen wurden. Es wird gezeigt, daß verbesserte Faltungs-
potentiale, die die Dichteabhängigkeit der effektiven Nukleon-
Nukleon-Wechselwirkung berücksichtigen, die α-Teilchen Streu-
querschnitte ohne jegliche Parameteranpassung gut beschreiben
können, auch für Streuwinkel weit oberhalb des Diffraktionsbe-
reichs. Bei der ^{6}Li-Streuung hingegen ist auch bei verfeinerter
Betrachtung - insbesondere des Überlappungsgebietes zwischen
Target und Projektil - eine Renormalisierung der Tiefe des
mikroskopisch berechneten Potentials notwendig, um die experi-
mentellen Wirkungsquerschnitte angemessen zu beschreiben.

The real parts of the optical model potentials for 104 MeV alpha-
particle and 156 MeV ^{6}Li ion scattering from ^{40,48}Ca are calcu-
lated in terms of folding model approaches. The validity of
different procedures is tested by comparing the predictions of
differential cross sectionswith experimental data measured
with high angular accuracy. It is found that a refined folding
potential accounting for density dependence of an effective
nucleon-nucleon interaction is appropriate for alpha particle
scattering without any parameters adjustment. However, for ^{6}Li
ion scattering renormalization of the depth of the real potential
is necessary.

1. INTRODUCTION

The optical model provides a general basis and powerful means for describing the interaction of nuclear particles involved in elastic scattering as well as in more complicated processes. A wide class of analyses of experimental data aims at a phenomenological determination of strengths, detailed shapes and energy dependence of the three nuclear components of the optical potential, the *real central, imaginary* and *spin-orbit* potential, the last term arising from the coupling between the spin and the orbital angular momentum of the incident particle. For complex particle scattering, studies of this type are concerned with the question of uniqueness of the potential shapes extracted from the experimental observations, that means with discrete and continuous ambiguities of the phenomenologically determined parameter values and with some "model dependence" due to the anticipated global forms used. Considering a particular case the question arises which radial parts of the potentials are sensitively probed by the scattering data and well determined by the measured differential cross sections covering a particular angular range at a particular energy of the projectile. These aspects have been discussed extensively in recent studies, especially for α-particle scattering /1,2/, considering also effects due to two-step processes like inelastic scattering, stripping and pick-up reactions /3/.

In principle, however, one would like to relate the optical potential to the fundamental nucleon-nucleon (NN) interaction, in an approach systematically including many-body corrections. Several such microscopic models have been worked out for nucleon-nucleus scattering as well as for scattering of complex projectiles. The essential ingredients of these approaches are the proton and neutron density distributions of the interacting particles and the nucleon-nucleon effective interaction in the medium of the two nuclei. Important steps in this direction have been

attempted by folding models, an approximation essentially based on the first term of a multiple scattering expansion of the (real part of) the optical potential.

There are basically two folding procedures. A single folding takes an adequate (semiempirical) nucleon-nucleus-1 potential and folds it into the density distribution of nucleus-2 /4,5/. A double-folding starts with an effective nucleon-nucleon interaction folded into the density of both nuclei /6,7,8/. Some phenomenological adjustments are usually necessary in order to obtain a satisfactory description of the experimental data and to reproduce the strength of the empirically determined real potential. Characteristically the heavy ion scattering folding models in their simplest form over-estimate the real potential in the vicinity of the strong absorption radius /9/. Such an observation may put the question to what extent we can trust the folding models to reproduce even the shape of the real potential or in which way we have to improve the approaches.

In addition to some possible over simplifications of the NN inter-action used by the calculations the main effects which are expected to modifiy substantially the calculated potential shapes are exchange terms and antisymmetrization /7,10/ and the density dependence of the nuclear interaction /12-15/. Of course, in so far we compare with experimental observations probing only a restricted part of the interaction potentials, the relative importance of such effects depends on the particular cases considered. With increasing overlap of the colliding particles the density dependence is expected to be more dominant while exchange contributions have been shown to be important in low energy scattering /16/.

In the present investigations we are concerned with these questions for the specific cases of 104 MeV α-particle scattering from ^{40,48}Ca and 156 MeV ^{6}Li scattering. Experimental studies of elastic scattering of intermediate energy α-particles /18,19/ have shown a definite filling of the Fraunhofer minima at large angles. That is interpreted to be due to refraction arising from the nuclear attraction. As discussed in detail by Goldberg et al. /19/ this behaviour enables the elimination of the discrete ambiguities in the phenomenlogically determined optical potentials, thus providing a more favourable situation for comparing phenomenologically derived potentials with folding model results. Less is known about the optical potentials for ^{6}Li scattering at medium high energy

above 100 MeV. Possibly this case may be characterized by
a transitional behaviour /20/ where the refractive phenomena
are considerably reduced due to the increased absorption estab-
lishing diffractive interactions, even in backward angle scat-
tering as similarily observed for scattering of heavier ions
/21/. Additionally the role of spin-orbit interactions has
to be explored, which may be done either in purely phenomenolo-
gical manner or applying semi-microscopic procedures /22/.
A serious examination of whether a spin-orbit interaction is
evident from the 156 MeV-^{6}Li scattering data is not in the
scope of the present paper. But we add some calculations with
phenomenological or simple "microscopic" forms of a spin-orbit
term in order to get a feeling on the influence of such a term
and its possible feed-backs to the discussion of the central
part.

Throughout in this paper our conclusions on the relative
importance of the effects included into the refined folding
model procedures (given in sects. 3 and 4) will be based on
the comparison with the phenomenological potentials and mea-
sured elastic scattering cross sections. It will be shown that
in the energy range under consideration exchange effects are
of less importance, but not completely negligible. Taking into
account density dependence, however, is essential. An adequate
treatment (sec. 4) will be able to reproduce the phenomenolo-
gical potentials correctly without the need of substantial
renormalization of the microscopically calculated values. This
particular result will fit into a current discussion /9, 40, 41/
of the adequate form of the effective interaction in heavy-ion
folding models.
Finally, an important aspect of the presented analyses arises
from recent attempts to extract nuclear size information, particu-
larily from α-particle scattering measurements, via folding model
approaches /17/.

2. EXPERIMENTAL DIFFERENTIAL CROSS SECTIONS AND PHENOMENOLOGICAL
    OPTICAL POTENTIALS

The experimental basis of our studies is provided by recent
experiments of elastic scattering of 104 MeV α-particles from
^{40,48}Ca /23,24/ and of 156 MeV ^{6}Li-ions from ^{40}Ca /25/.
As the angular distributions are affected by the phenomena

considered only through very little shifts of the general diffrac-
tion pattern and other small variations (e.g. deepness of the
minima and steepness of the overall slope) precise and accurate
determinations of the angular distributions are a quite necessary
prerequisite of any reasonable conclusions from comparison of
theory and experiment. For this,the differential cross sections
have been carefully measured with high angular accuracy up to
the angular region where the diffraction pattern is strongly
damped, in the case of ^{40,48}Ca (α,α) into the region of the
exponential fall-off (beyond the nuclear rainbow angle) of
σ/σ_{Ruth}. Fig. 1 presents the measured cross sections. Experi-
mental details are given elsewhere /24,25/.

The best way avoiding the constraint of phenomenological
parametrizations of the optical potentials would be an application/45/
of "model independent techniques" originally worked out for
electron scattering analyses. Such a technique has been recently
applied to the present ^{40,48}Ca (α,α) data revealing lucidly
the uncertainties of each radial point of the potential distribu-
tion /23/. It turns out that the resulting distributions can be
fairly well parametrized by a *squared* Saxon-Woods form. In fact,
comprehensive investigations of elastic α-particle scattering
which cover a wide energy range and a representative number of
target nuclei /11/ have demonstrated that the squared Saxon-Woods
form-factors provide a more appropriate representation of the
shape of the α-particle scattering optical potentials rather
than the usual standard Saxon-Woods form. Our phenomenological
analysis follows the suggestions of such results and uses an
optical potential V + iW parametrized by

$$V(r) = U_V \left[1 + \exp\left(\frac{r-D_1}{d_1}\right)\right]^{-2} \tag{2.1a}$$

$$W(r) = W_V \left[1 + \exp\left(\frac{r-D_2}{d_2}\right)\right]^{-2}$$
$$+ 4\, d_3\, W_s\, \frac{d}{dr}\, \left([1 + \exp\left(\frac{r-D_3}{d_3}\right)]\right)^{-2} \tag{2.1b}$$

The Coulomb potential has been generated by a uniformly charged
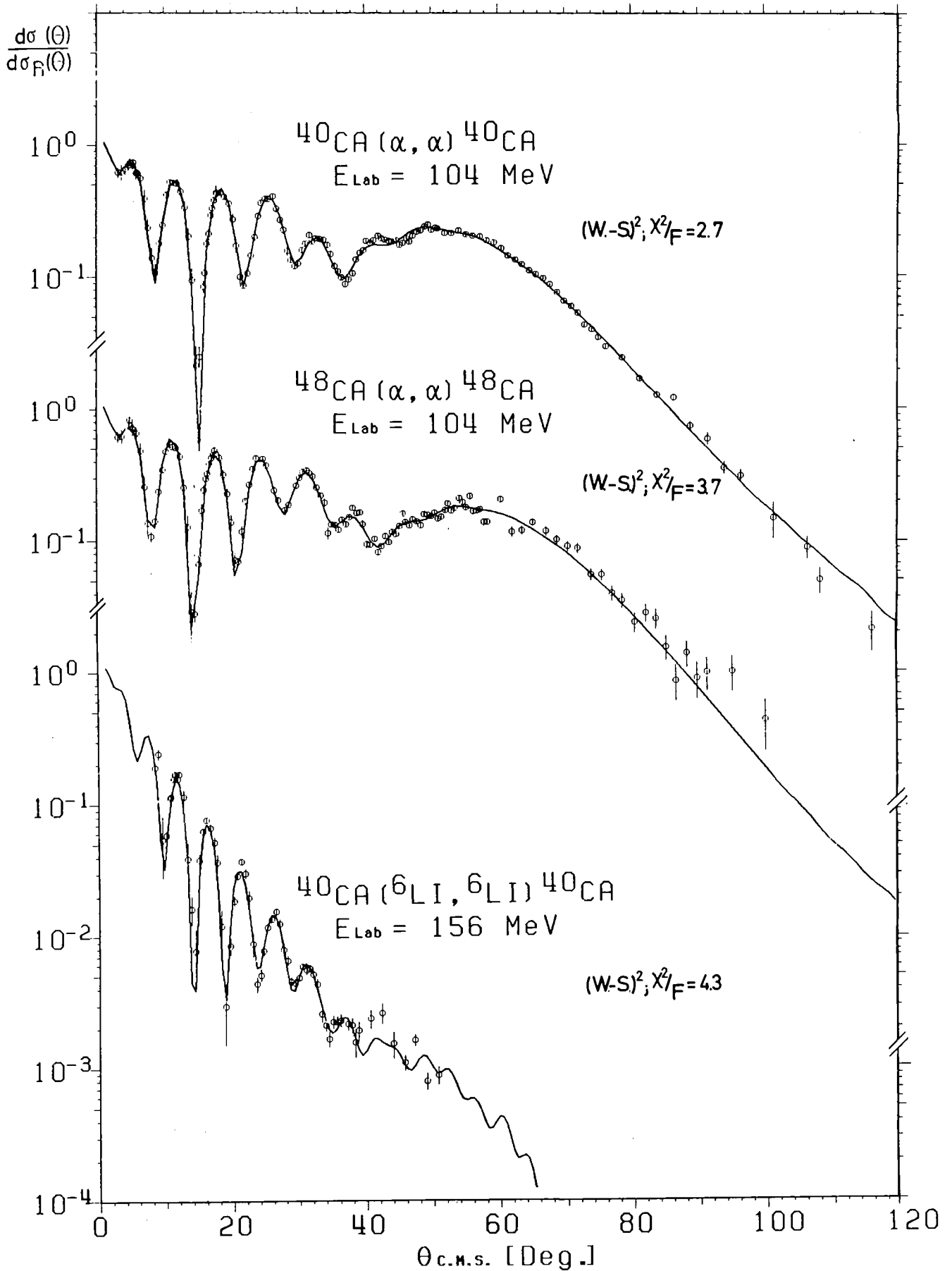sphere with radius $R_c = 1.34\ A^{1/3}$ fm.

Fig. 1   Elastic scattering of 104 MeV α-particles and 156 MeV
^{6}Li ions. Experimental differential cross sections as
compared to optical model calculations using a *squared*
Saxon-Woods form of the potentials.

The parameter values have been adjusted by an automatic search routine minimizing χ^2 per degree of freedom. The results are compiled in tab. 1 and displayed in fig. 1. The real and imaginary parts of the resulting α-^{40}Ca and one of the ^{6}Li-^{40}Ca potentials are shown in fig. 2. Obviously surface absorption contributes considerably in the case of α-particle scattering.

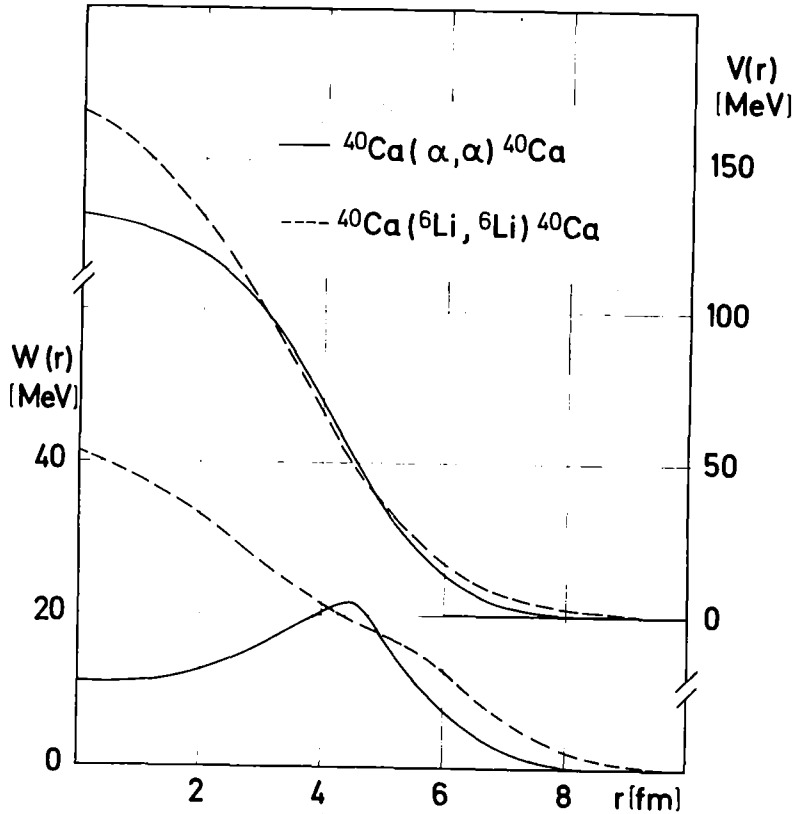Fig. 2: Shapes of the real and imaginary parts of the phenomenological α-^{40}Ca and ^{6}Li-^{40}Ca potentials.

In ^{6}Li scattering several equivalent potential families have been found. Following corresponding considerations of the energy denpendence of α-particle scattering potential /5/ we estimate

$$V(r=0) = \left[3 \, V^{o}_{Prot} \, (r=0) + 3 \, V^{o}_{Neut} \, (r=0) \right] \left[1 - \frac{dV}{dE}(\bar{E}_N + E) \right] \qquad (2.2)$$

with V^{o}_{Prot} and V^{o}_{Neut} the nucleon-target optical potentials at zero energy, $\bar{E}_N$ representing the mean kinetic energy of a nucleon in the ^{6}Li-ion and $E = E_{Li}/6$. This relation favours the potential families around $V(r=0) \simeq 180$ MeV.

Including a spin-orbit potential $U_{SO} = U_S \frac{1}{r} \frac{df(r)}{dr}$ with $f(r)$ similar to the central form factor does not vary the results significantly.

Table 1. Phenomenological optical potentials: Parameter values of the best fit.

	U	$D_1 \cdot A_T^{-1/3}$	d_1	$<r^2>_U^{1/2}$	J_N	W_v	$D_2 \cdot A_T^{-1/3}$	d_2	N_S	$D_3 \cdot A_T^{-1/3}$	d_3	χ^2/F
	(MeV)	(fm)	(fm)	(fm)	(MeV fm^3)	(MeV)	(fm)	(fm)	(MeV)	(fm)	(fm)	
$^{40}Ca(\alpha,\alpha)$	135.2	1.480	1.144	4.318	326.8	11.34	1.801	1.349	11.4	1.440	0.840	2.7
$^{48}Ca(\alpha,\alpha)$	145.3	1.431	1.166	4.422	317.5	13.66	1.776	1.172	9.42	1.414	0.834	3.7
	260.6	1.255	1.599	4.457	278.9	50.96	1.515	1.915	5.17	1.763	0.933	4.3
^{40}Ca	234.0	1.323	1.512	4.458	283.0	41.33	1.666	1.857	5.37	1.770	0.796	4.6
$(^6Li,^6Li)$	185.0	1.356	1.612	4.627	242.9	47.47	1.490	1.962	4.86	1.837	0.861	5.3
	132.1	1.488	1.507	4.722	219.9	70.95	1.360	2.052	2.39	1.958	0.816	6.5

3. ANTISYMMETRIZATION AND DENSITY DEPENDENCE EFFECTS IN FOLDING MODEL POTENTIALS

a. Theoretical Procedure

There are numerous attempts of microscopic descriptions for the interaction of composite particles with nuclei, and several different procedures with increasing sophistication have been worked out, in particular for α-particle scattering /4-8,26/. Most calculations are carried out by folding into the target nucleus density distribution ρ_T an effective α-particle-bound-nucleon interaction V_{P-N_T} (R_P) which is either taken from phenomenological analyses of nucleon-α-particle scattering at low energy /27/ or itself generated by folding a nucleon-nucleon interaction into the α-particle density distribution ρ_P /28/

$$U_{PT}^{(P)} (r) = \int d \vec{z}_T \, \rho_T \, (\vec{z}_T) \, V_{P-N_T} \, (\vec{R}_P) \qquad (3.1)$$

The latter method is equivalent to a double folding procedure /6/ calculating the leading (simple direct) term of the real part of the optical potential by

$$U_{PT}^{(S)} (r) = \int\int d\vec{z}_P d\vec{z}_T \, \rho_P (\vec{z}_P) \rho_T (\vec{z}_T) \, t(\vec{r}_{NN}) \qquad (3.2)$$

where the coordinates used are defined in fig. 3. The quantities ρ_P and ρ_T are matter point density distributions of the projectile and the target nucleus, respectively, $t(\vec{r}_{NN})$ is an effective nucleon-nucleon interaction assumed to be density independent in simple calculations. Eq. (3.2) neglects noncentral terms and isospin dependence in the nucleon-nucleon potential.
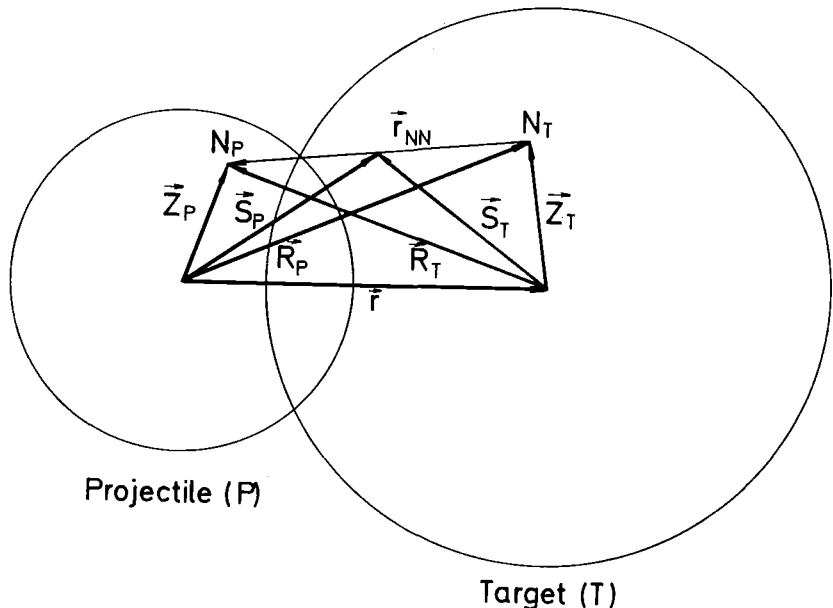

Fig. 3: Coordinates of the Projectil-Target-System

Projectile (P)

Target (T)

Moreover exchange and antisymmetrization effects due to the Pauli principle are omitted. On the other hand, single folding procedures using phenomenological projectile-nucleon potentials /27/ or phenomenologically adjusted effective interactions /28,29,30/, sometimes supplemented by an energy-dependent pseudo-potential accounting for exchange effects /10,31/, implicitely absorb a great of the neglected effects. This may explain why actually single folding models proved to be more successful in describing experimental data when compared to the simple double folding procedure of the type of eq. 3.2.

Alternatively to the folding over the target density ("target folding") by eq. 3.1 a single folding procedure ("projectile folding") may start with an adeqaute nucleon-target nucleus interaction V_{T-N_P}, then constructing the real part of the projectile-target interaction by integrating over the complex projectile density distribution /5,32/

$$U_{PT}^{(T)} (r) = \int d\vec{z}_P \; \rho_P(\vec{z}_P) \; V_{T-N_P} (R_T) \qquad (3.3)$$

In the present investigation we attempt to construct more refined complex projectile-bound (target) nucleon V_{P-N_T} and nucleon-target nucleus V_{T-N_P} interactions starting from a realistic nucleon-nucleon force and including antisymmetriza- tion and density dependence of the interaction. We follow the approach of Majka et al. / 7 / worked out for a double folding model of the alpha-target interaction. Considering the complex projectile - target potential one has to note that the influence of exchange and of the density dependence is included merely in V_{P-N_T} and V_{T-N_P}, respectively so that the two procedures (eqs. 3.1 and 3.3) may differ in the results. It seems to be interesting to compare both ways with each other and to the simple direct potential (calculated with the density independent part of the NN interaction).

The projectile-bound-nucleon V_{P-N_T} and nucleon-target V_{T-N_P} potentials are deduced from a density dependent effective

nucleon-nucleon interaction t_ρ by including antisymmetrization effects in the form

$$V_{P-N_T}(\vec{R}_P) = \int d\vec{z}_P \rho_P(\vec{z}_P)\, t_\rho(r_{NN}) \qquad (3.4a)$$

$$+ \frac{1}{2} \sum_{i=n,p} \int d\vec{z}_P \rho_P^{Mix}(\vec{R}_P,\vec{z}_P)\, t_\rho(r_{NN})\, j_0(r_{NN}k_{iT})$$

and in an analogous form

$$V_{T-N_P}(\vec{R}_T) = \int d\vec{z}_T \rho_T(\vec{z}_T)\, t_\rho(r_{NN}) \qquad (3.4b)$$

$$+ \frac{1}{2} \sum_{i=n,p} \cdots$$

The quantities ρ_{Mix} are mixed densities originating from the nonlocal exchange part of the potential, resulting from antisymmetrization requirements. They are calculated by a modification of the Slater approximation /33/ due to Pandharipande /34/. The effective nucleon-nucleon interaction is introduced by the form

$$t_\rho^{np} = \frac{1}{8}(t_{SE} + 3\, t_{TE}) \qquad (3.5)$$

$$t_\rho^{pp} = \frac{1}{4}\, t_{SE}$$

The singlet t_{SE} and triplet t_{TE} s-state effective interaction are more explicitely expressed by

$$t_i(r_{NN}) = c_i\left[1 + \alpha_i \rho_{P(T)}^{2/3}(\vec{s}_{P(T)})\right] v_{KK}^i(r_{NN}) \qquad (3.6)$$

where v_{KK}^i are the singlet and triplet state potentials given by Kallio and Kolltveit/35/ with Moszkowski-Scott separation distances 1.025 fm and 0.925 fm, respectively. The values of the parameters c_i and α_i are taken from ref./36/. The wave numbers k_{ix} in the argument of the zero-order Bessel function are taken at $\vec{s}_y = \frac{1}{2}(\vec{R}_y + \vec{z}_y)$ and are given for proton (p) and neutron (n) by

$$k_{px}(\vec{s}_y) = \{\frac{2m}{h^2} \left| E_{N_x}^{CM} - V_{y-px}(\vec{s}_y) + V_c(\vec{s}_y) \right| \}^{1/2} + <k_{int_x}> \qquad (3.7)$$

$$k_{nx}(\vec{s}_y) = \{\frac{2m}{h^2} \left| E_{N_x}^{CM} - V_{y-nx}(\vec{s}_y) \right| \}^{1/2} + <k_{int}>_x$$

(x=P(T) , y=T(P))

with $E_{N_x}^{CM}$ and m standing for the center of mass energy and reduced mass in nucleon-nucleus system, V_c for the Coulomb potential. The quantity $<k_{int,x}>$ is the wave number corresponding to the average internal momentum of the nucleon x in the nucleus in which it is immersed. Eqs. (3.4) have been resolved iteratively. The resulting nucleon-target and projectile-target nucleon potential are energy dependent via eqs. (3.7).

Noting again that any influence of a density dependence of the nucleon-nucleon force is included only in the first step calculating the projectile-bound target nucleon and target-projectile nucleon interaction, respectively,and taking t_ρ for the density values of the non-interacting particles, the approach implies that a pronounced density compression does not occur in the overlap region of the colliding nuclei. The influence of this "adiabatic" approximation is compared to a "sudden" approximation in sec . 4 including some improvement in the treatment of the problem.

b.   RESULTS FOR 104 MeV α-PARTICLE SCATTERING ON $^{40,48}Ca$

In the actual calculations the matter point density distribution of the α-particle is represented by a Gaussian form with parameter values taken from ref. /37/. Presuming that proton and matter distributions in ^{40}Ca are identical, a three-parameter Fermi shape is used as extracted from measured charged density distribution by unfolding the charge density

distribution of a single proton /51/. From experimental investigations using electromagnetic probes /38,39/ we know that the proton distributions in ^{40}Ca and ^{48}Ca nuclei are very similar and do not differ in the values of the rms radii while the neutron distribution in ^{48}Ca is object of considerable experimental and theoretical efforts /17/. In the present calculations we start with the matter distribution ρ_m of ^{48}Ca to be identical to the proton distribution ρ_p, and it will turn out that the experimental data do require an increased rms radius of the neutron distribution ρ_n in ^{48}Ca.

Fig. 4 displays the real part of the α-particle-^{40}Ca potential calculated by the different procedures which we like to compare. In tab. 2 the potentials are characterized by the central depths U_{PT} $(r = o)$, the rms radii $<r^2>^{1/2}$ and volume integral J_N per nucleon. Though the microscopic potentials cannot be represented adequately by a Saxon-Woods form, values for a half-way radius and a 10-90 % distance t_{10-90} are given, too. It is obvious that the density dependence of the NN interaction and exchange effects influence the shapes considerably.

Applying the microscopic potentials for the description of the measured differential cross sections of elastic scattering one has to add an imaginary part iW (see eq. 2.2) in a phenomenological way as it is common praxis. Moreover, a normalization factor λ_R for the depth of the real potential has to be introduced since it is obvious from comparison with the results from phenomenological analysis that the microscopic calculations do not reproduce the experimentally required values U(r) in the correct scale. The values of the parameter λ_R and of the parameters describing the imaginary part adjusted by an automatic search routine on the basis of a χ^2/F criterion are given in tab. 3. The resulting theoretical cross sections are presented by fig. 5. Additionally, in order to notify and separate effects arising from density dependence and those from exchange microscopic potentials with and without
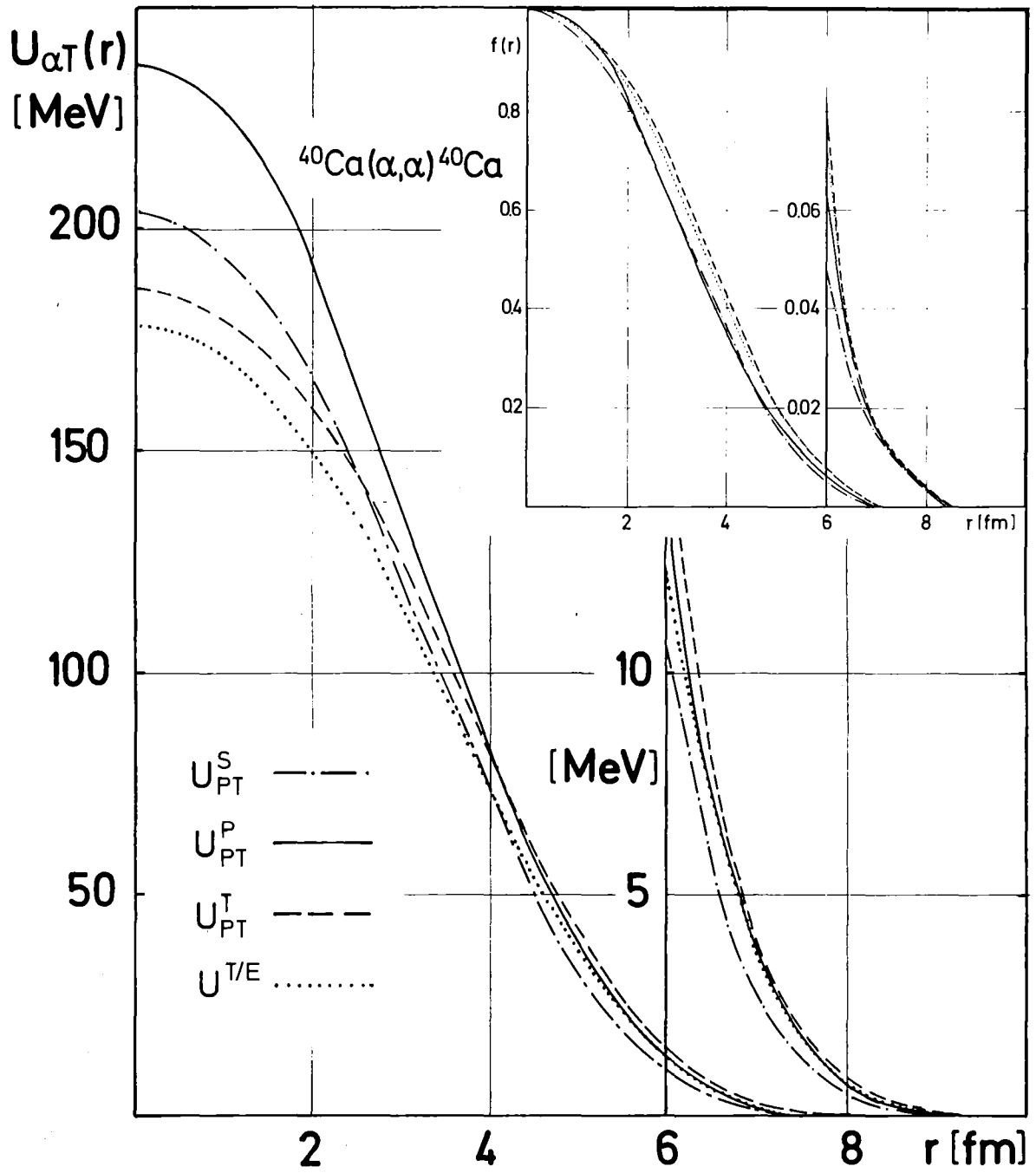
Fig. 4: Microscopic α-particle-^{40}Ca potentials calculated using different approaches.

Inset: Form factors of presented potentials.

Table 2. Parameters of the real part of the microscopic
α-particle-^{40}Ca potentials.

Approach	$U_{PT}(r=0)$ (MeV)	$<r^2>^{1/2}$ (fm)	J_N (MeV fm^3)	$R_{1/2}$ (fm)	t_{10-90} (fm)
S	203.3	4.084	346.9	3.352	3.980
P	237.6	4.015	400.4	3.327	4.089
T	186.2	4.246	393.9	3.726	4.093
T/E	178.1	4.247	360.7	3.618	4.148

S: Simple direct potential (eq. 3.2).

P: Antisymmetrization and density dependence effects are
included in the nucleon-projectile system (eq. 3.3 and 3.4 a).

T: Antisymmetrization and density dependence effects are
included in the nucleon-target system (eq. 3.1 and 3.4 b).

E: Antisymmetrization effects are neglected.

antisymmetrization term in eq. 3.4b have been calculated and
are compared in their shapes and influences on the theoretical
cross sections. Obviously the exchange effect modifies the shape
of the potential in a minor way than the density dependence of
the NN interaction.

Tab. 4 and 5 compile the results of the microscopic analyses
of ^{48}Ca (α,α). Corresponding theoretical cross sections are
shown in fig. 6. Recently, it has been attempted to extract the
neutron distribution ρ_n from the ^{48}Ca (α,α) data /23/ by use
of a more or less phenomenological α-bound-nucleon interaction
$V_{\alpha-N_T}$, empirically adjusted in the case ^{40}Ca (α,α) ^{40}Ca. It has
been found that the rms radius of the neutron distribution is
slightly larger than the value of the proton distribution, in
agreement with other results (see ref./23/).Introducing this
neutron distribution into our calculations reproduces the experi-
mental cross sections clearly better than the assumption $\rho_n \equiv N/Z \cdot \rho_p$.

Table 3. Optical model best fit parameters for ^{40}Ca (α,α) ^{40}Ca scattering. Corresponding theoretical differential cross sections are shown in fig. 5.

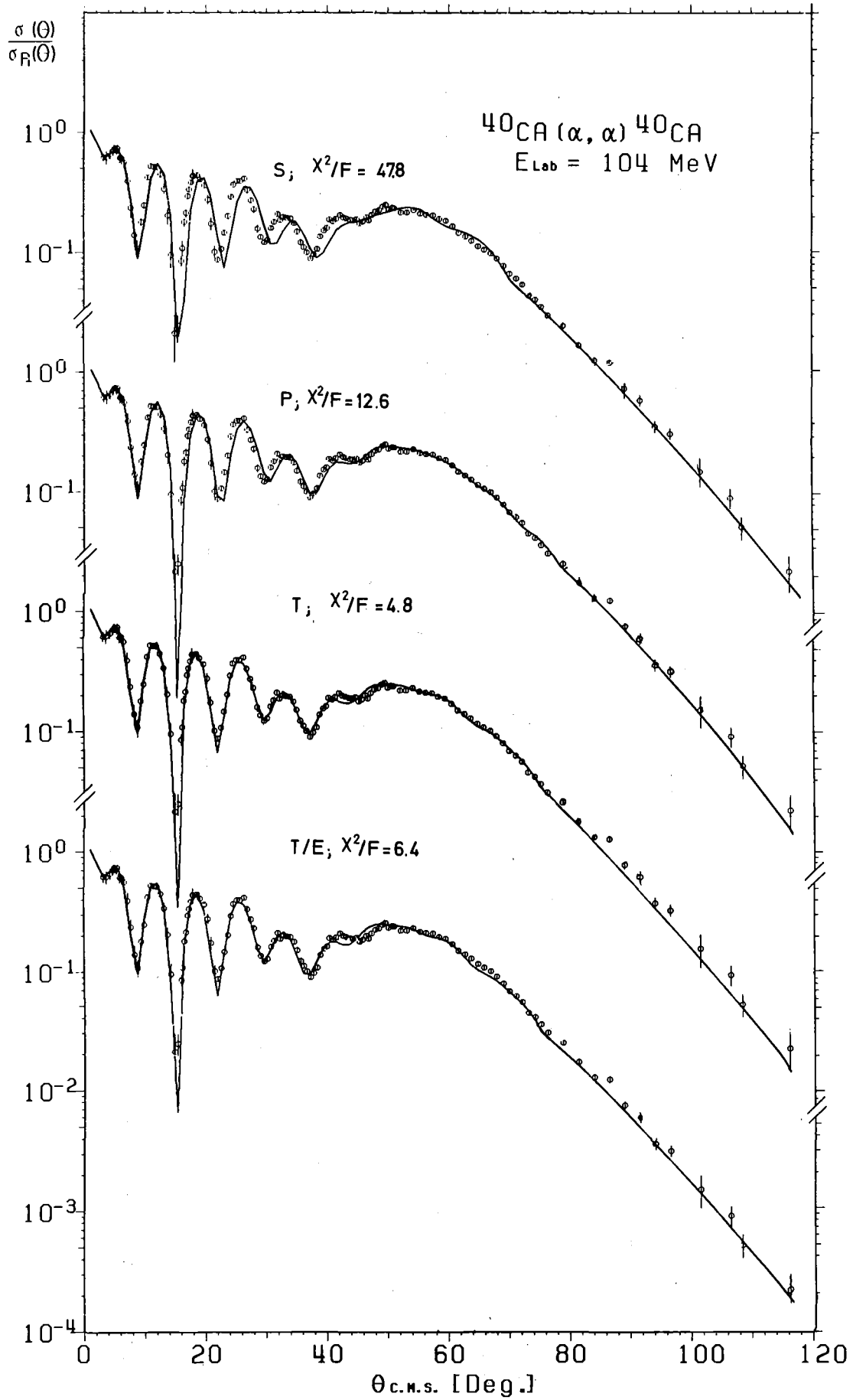| Real Potential Approach[+]	λ_R	W_v (MeV)	$D_2 \cdot A_T^{-1/3}$ (fm)	d_2 (fm)	W_s (MeV)	$D_3 A_T^{-1/3}$ (fm)	d_3 (fm)	χ^2/F
S	0.791	2.59	2.230	0.607	18.61	1.190	0.925	21.2
P	0.685	10.93	1.949	1.083	11.06	1.151	0.728	12.6
T	0.791	11.49	1.760	1.402	10.03	1.328	1.166	4.8
T/E	0.848	10.24	1.993	1.141	10.76	1.242	0.838	6.4

[+] See explanations in table 2.

-15-

Fig. 5: Optical model fits to the $^{40}Ca(\alpha,\alpha)^{40}Ca$ cross sections using various approaches for the real folded potential.

Table 4. Parameters of the real part of the microscopic
α-particle-^{48}Ca potentials

Approach[+]	$U_{P-T}(r=0)$ (MeV)	$<r^2>^{1/2}$ (fm)	J_N (MeV fm^2)	$R_{1/2}$ (fm)	t_{40-90} (fm)
S	238.4	4.074	346.3	3.415	3.920
T	203.6	4.269	370.9	3.793	4.092
T/N[++]	195.6	4.397	384.3	3.878	4.205

[+] See explanations in table 2.

N[++]: Neutron density distribution $\rho_n \neq \rho_p$, taken from ref./23/.

In fig. 7 the phenomenologically determined optical potential (real part) for α-particle-^{48}Ca scattering (tab.1) is compared to the microscopic potentials of tab. 4 renormalized by the corresponding λ_R-value of tab. 5. It is evident that in the region which is probed by elastic scattering refined α-particle scattering folding models are able to predict the potential shape.

Finally, in fig. 8 we compare the microscopically calculated α-particle-*free*-nucleon interaction $V_{\alpha-N_T}$ /42/ which we need for proceeding via eq. 3.1 with that which has been phenomenologically extracted from ^{40}Ca (α,α) ^{40}Ca scattering assuming $\rho_n = \rho_p$ in ^{40}Ca /23/. The phenomenological derived interaction is parametrized by a modified Fermi form $V_0(1 + \omega r^2/R_\alpha^2)$ $(1 + \exp((r-R_\alpha)/a)^{-1,723}$ with $V_0 = 39.28$ MeV, $R_\alpha = 1.557$ fm, $a = 0.894$ fm, $\omega = 0.132$. This interaction absorbs implicitely some effects resulting from target nucleus and therefore both interactions differ considerably.

Table 5. Optical model best fit parameters for ^{48}Ca (α,α) ^{48}Ca scattering. Corresponding theoretical differential cross sections are shown in fig. 6.

Real Potential Approach[+]	λ_R	W_v (MeV)	$D_2 A_T^{-1/3}$ (fm)	d_2 (fm)	W_s (MeV)	$D_3 A_T^{-1/3}$ (fm)	d_3 (fm)	χ^2/F
S	1.044	4.80	2.143	0.747	35.72	1.238	0.534	21.3
T	0.772	5.24	2.080	0.811	18.77	1.229	0.745	10.9
T/N[++]	0.793	17.68	1.772	1.358	12.68	1.322	0.423	6.4

[+] See explanations in table 2.

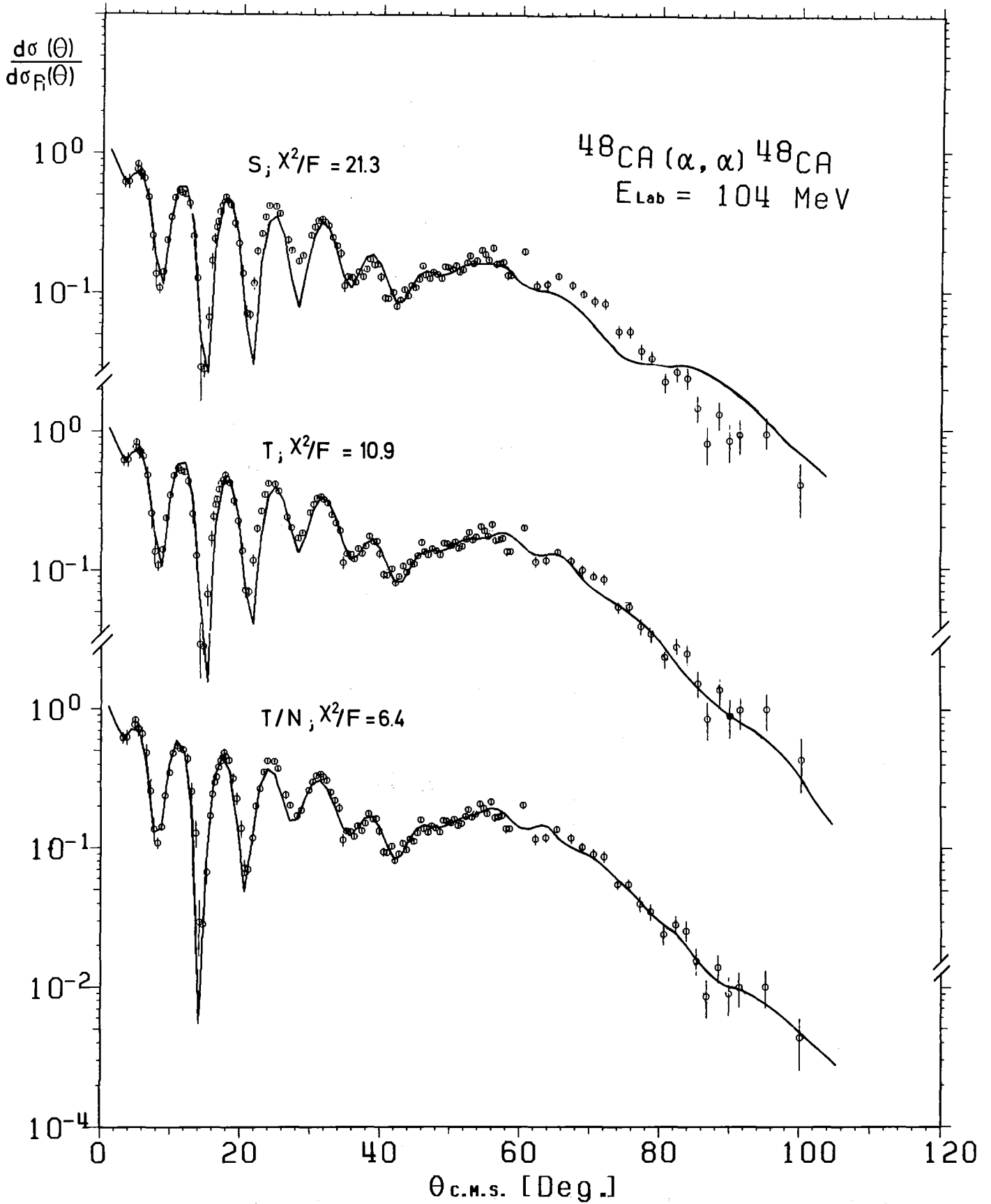N[++]:Neutron density distribution $\rho_n \neq \rho_p$, taken from ref. 23.

Fig. 6: Optical model fits to the ^{48}Ca$(\alpha,\alpha)^{48}$Ca cross sections using various approaches for the real folded potential.
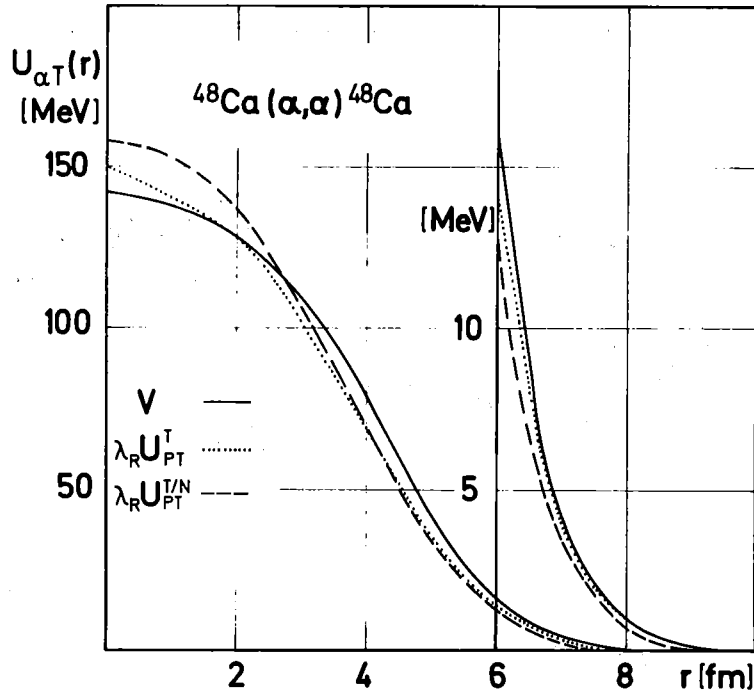
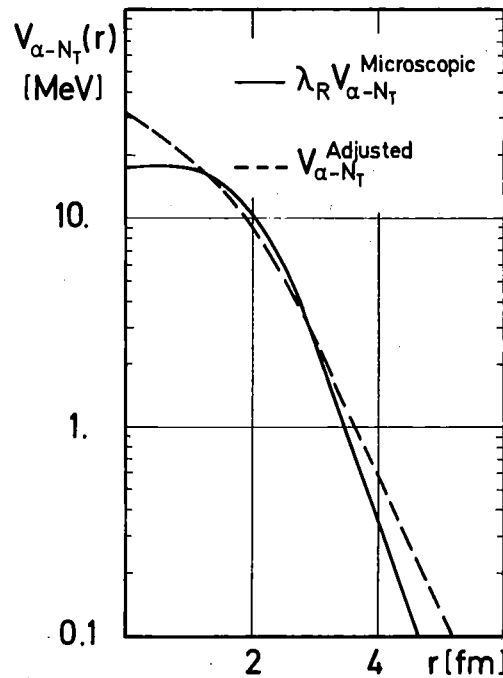Fig. 7 Comparison of the real part of the α-particle-^{48}Ca
optical potentials.

Fig. 8 Microscopic α-particle-*free*-nucleon interaction
$V_{\alpha-N_T}$ (renormalized by the factor λ_R = 0.685)
as compared to a phenomenologically interaction
empirically derived from ^{40}Ca (α,α) ^{40}Ca at E_α = 104 MeV.

c. Results for ^{6}Li-^{40}Ca-Scattering

The microscopic ^{6}Li-^{40}Ca potential have been calculated
with a two-parameter Fermi shape of the density distribution
in ^{6}Li deduced from ref. /43/. The results of the various proce-
dures are given in tables 6 and 7. The corresponding theoretical

Table 6. Parameters of the real part of the microscopic ^{6}Li-^{40}Ca
          potentials.

Approach[+]	$U_{PT}(r=0)$ (MeV)	$\langle r^2 \rangle^{1/2}$ (fm)	J_N (MeV fm^3)	$R_{1/2}$ (fm)	t_{10-90} (fm)
S	245.5	4.472	344.1	3.424	4.429
P	370.6	4.248	483.4	3.427	4.514
T	242.8	4.616	390.7	3.729	5.572

[+] See explanations in table 2.

cross sections calculated similarily to the α-particle scattering
case are displayed in fig. 9. In Fig. 10 again we compare the
phenomenologically determined optical potential for ^{6}Li-^{40}Ca
scattering (tab. 1) with the microscopic potentials, renormalized
by the phenomenological parameter λ_R (tab. 7). The inset in
fig. 10 shows the shape of the microscopically calculated ^{6}Li-
bound nucleon interaction V_{Li-N_T} which can be fairly well para-
metrized by a modified Fermi form (see sect. 3 b) /42/ with
$V_o \equiv 36.6$ MeV for ($E_{Li} = 156$ MeV) $R_{Li} = 2.408$ fm a = 0.908 fm
and ω = - 0.039 and the exponent m = 1.351.

Table 7. Optical model best fit parameters for ^{40}Ca $(^6Li,^6Li)$ ^{40}Ca scattering. Corresponding theoretical differential cross sections are shown in fig. 9.

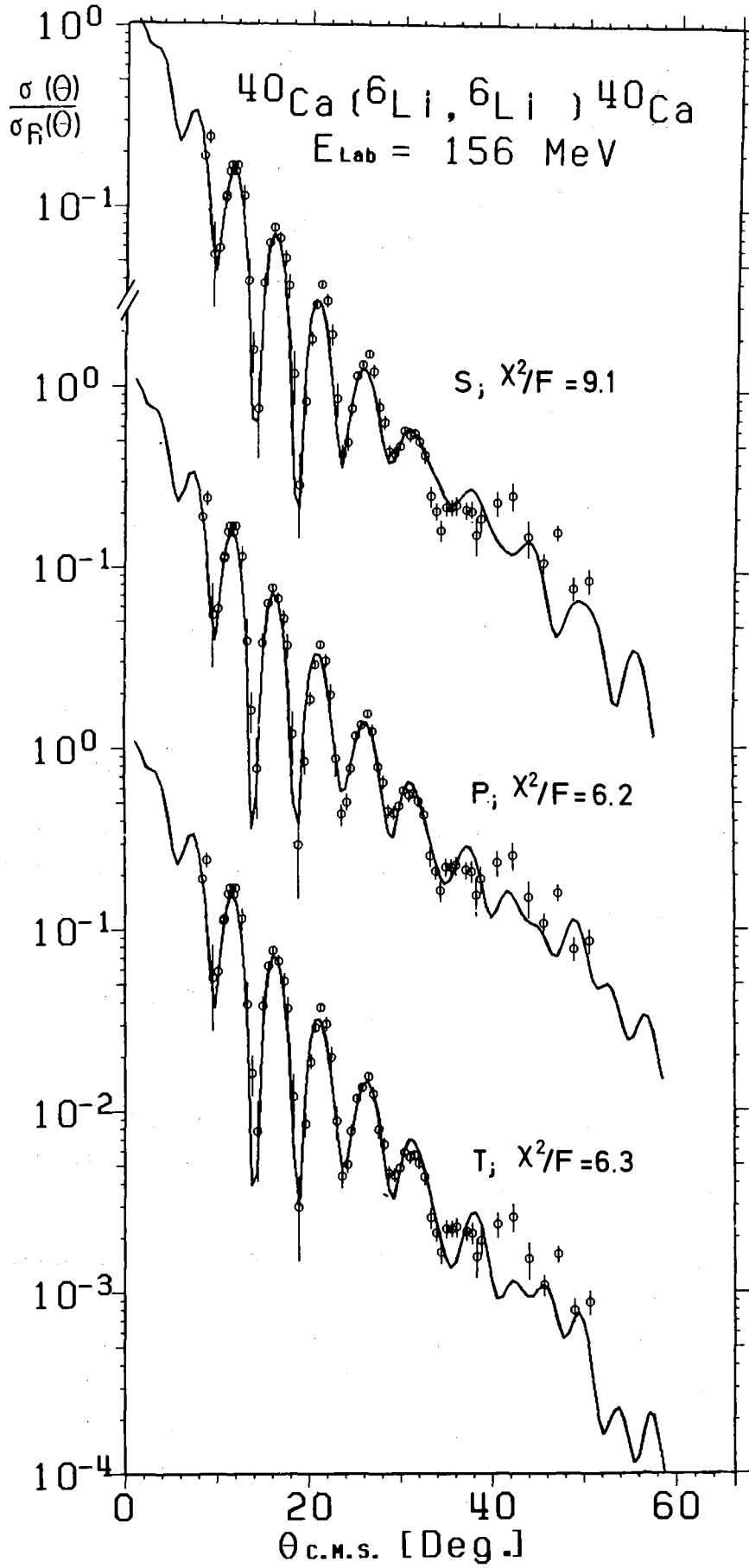| Real Potential Approach[+]	λ_R	W_V (MeV)	$D_2 \cdot A_T^{-1/3}$ (fm)	d_2 (fm)	W_s (MeV)	$D_3 \cdot A_T^{-1/3}$ (fm)	d_3 (fm)	χ^2/F
S	0.767	29.50	1.531	0.348	16.30	1.499	1.655	9.1
P	0.505	61.13	1.463	2.029	3.41	1.866	0.751	6.2
T	0.604	49.51	1.438	2.168	5.14	1.841	0.824	6.3

[+] See explanations in table 2.

Fig. 9: Optical model fits to the $^{40}Ca(^6Li,^6Li)^{40}Ca$ cross sections using various approaches for the real folded potential.
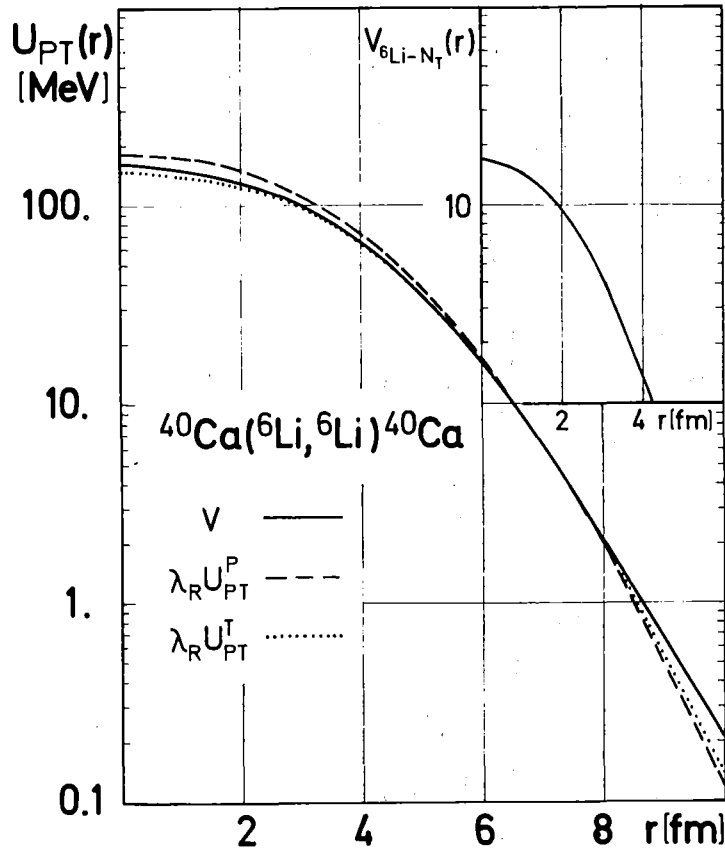
Fig. 10 Shapes of the real part of the phenomenological
and microscopic potentials (projectile folding re-
normalized by λ_R from tab. 7) for ^6Li-^{40}Ca scatte-
ring.

Inset: Shape of $\lambda_R \cdot V_{Li-N_T}$ (λ_R = 0.505).

4. IMPROVED TREATMENT OF THE DENSITY DEPENDENCE OF THE NN-INTERACTION: SUDDEN AND INTERMEDIATE APPROXIMATION

In addition to the purely phenomenological handling of the
imaginary part of the optical potential the need of empirical
renormalization of the microscopically calculated potentials
(by factors λ_R < 1) is origin of considerable criticism of the
folding models, especially for heavy ion scattering /9/ and it
indicates unsufficient inderstanding of important contributions.

Recently, a more refined NN interaction in the framework of a double-folding model of heavy ion scattering has been proposed which seemed to reproduce the real potentials at the strong absorption radii correctly /40/. Although successful in several cases, this form of interaction is actually not able to remove the discrepancies in α-particle and ^{6}Li scattering /41/. In view of the results in the preceding sections a more detailed discussion of the density dependence may shed some light on the problem. In fact, it has been pointed out that the failure of the single folding model to predict the correct real HI potential is partially due to omission of density dependence effects /44/.

For the ensuring studies we neglect the antisymmetrization term in eq. 3 (justified by the results in tab. 3) and calculate the optical potential by

$$U_{PT}(r) = \int d\vec{z}_P \, \rho_P(\vec{z}_P) \int d\vec{z}_T \, \rho_T(\vec{z}_T) t_\rho (\vec{r}_{NN}, \rho) \qquad (4.1)$$

In a local density approximation the density ρ appearing in t_ρ may be given by

$$\rho = m \cdot \rho_P (\vec{z}_P + r_{NN}/2) + \rho_T (\vec{z}_T + r_{NN}/2) \qquad (4.2)$$

so that the inner integral of eq. 4.1 which for m=0 (or the "adiabatic" approximation used in sect. 3) is just the free-nucleon target potential, is now dependent on the density ρ_P of the imbedded projectile nucleons. The factor $m (0 \leq m < 1)$ accounts for the degree of the compressibility of the nuclear matter in the overlap region of the colliding nuclei. Thus, the singlet and triplet interaction is more explicitely written

$$t_i(r_{NN}) = c_i \{1-\alpha_i [m; \rho_P (\vec{z}_P+\vec{r}_{NN}/2)+\rho_T(\vec{z}_T+\vec{r}_{NN}/2)]^{2/3}\}v_{KK}^i$$

$$= g_i(\rho)v_{KK}^i(r_{NN}) \qquad (4.3)$$

In order to simplify the calculations we neglect $r_{NN}/2$ in the arguments of ρ_P and ρ_T and do use a more convenient parametrization of the density dependence by

$$g_i(\rho) = \beta_i \exp(-\gamma_i\rho) - \delta \exp(\varepsilon_i\rho) \qquad (4.4)$$

This parametrization* represents very well the form in
eq. 4.3 (see fig. 11) for density values ρ under consideration.

In order to get a feeling of the influence of the various
approximations we compare the calculated nucleon-target poten-
tials (the inner integral of eq. 4.1) resulting from following
procedures

a. neglecting the density dependence ($g_i(\rho) = 1$)
b. including the density dependence in the exact form
    of eq. 4.3
c. including the density dependence in the form of
    eq. 4.3, but neglecting $\vec{r}_{NN}/2$ in the argument of ρ_T.
d. introducing the parametrization given by eq. 4.4 and
    neglecting $\vec{r}_{NN}/2$ in the argument of ρ_T.

The results displayed in fig. 12 show that the depth of
the resulting potential is affected to few percent by the
approximation dropping $\vec{r}_{NN}/2$ in the argument of ρ_T.

The results of the calculations of the α-particle-^{40}Ca
and ^{6}Li-^{40}Ca potentials (eq. 4.3) using the approximations
discussed, chosing m=1 ("sudden" approximation) and fitting the
experimental cross sections (see sect. 3.6) are given in
tab. 8. For α-particle scattering the best fit requires a
normalization factor $\lambda_R > 1$ indicating some overestimation
of the saturation effects in the case of m=1, while the adjust-
ment of m=0.5 implies just $\lambda_R = 1$ for the best fit (see tab. 9).
On the other hand, for ^{6}Li-scattering, even by the "sudden" approxima-

---

*The more familiar form $(1-2\rho^{2/3})$ /46/ can be represented by
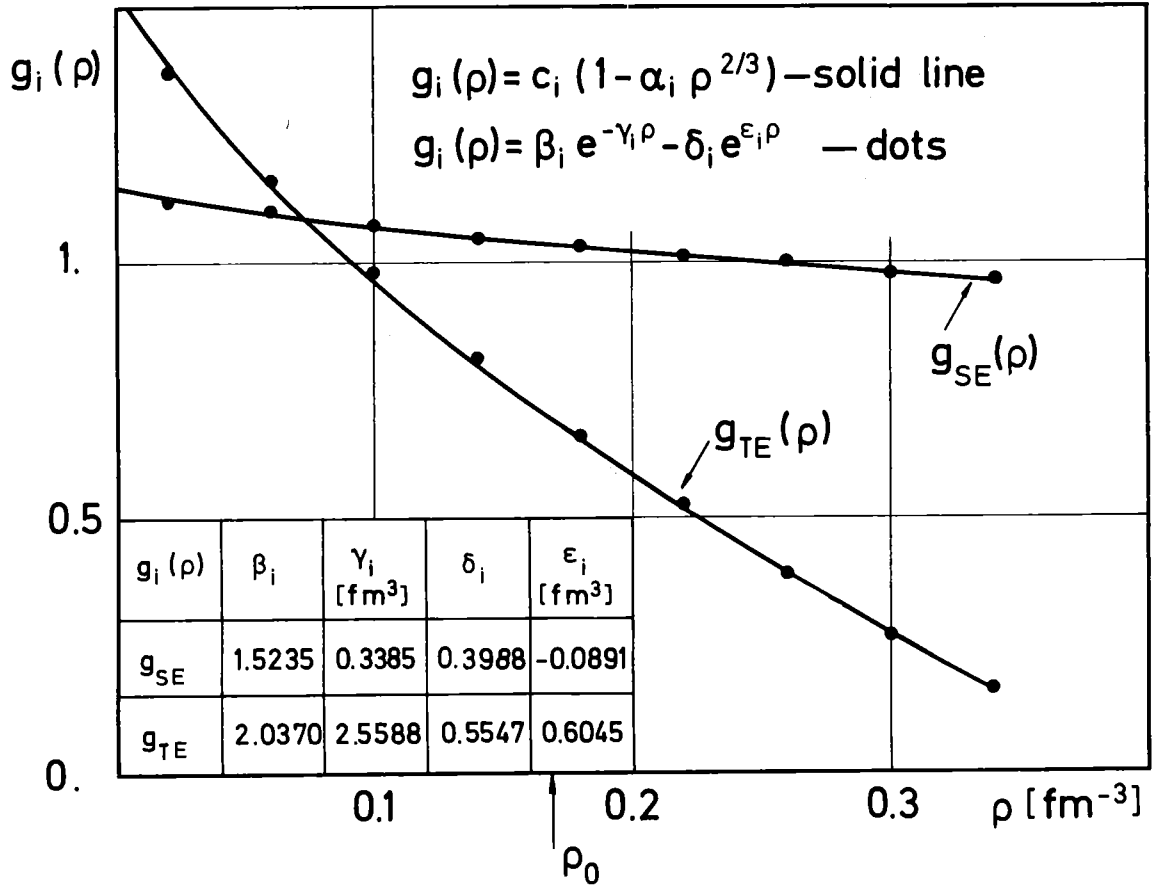 eq. 4.4 with β=1.2813, γ = 2.6966, δ = 0.3742 and ε = 0.7394.

Fig. 11 Different representations of the density dependence of the NN interaction.

Tab. 8 Parameters of the real part of the microscopic α-^{40}Ca and ^{6}Li-^{40}Ca potentials

	Approach*	$U_{PT}(r=0)$ (MeV)	$<r^2>^{1/2}$ (fm)	J_N (MeV fm3)	$R_{1/2}A_T^{-1/3}$ (fm)	t_{10-90} (fm)
^{40}Ca(α,α)	SD	124.9	4.25	249.6	1.047	4.17
	IM	151.4	4.22	298.0	1.046	4.10
^{40}Ca$(^{6}$Li,^{6}Li)	SD	201.3	4.62	310.0	1.056	4.60

*SD-sudden approximation (m=1)

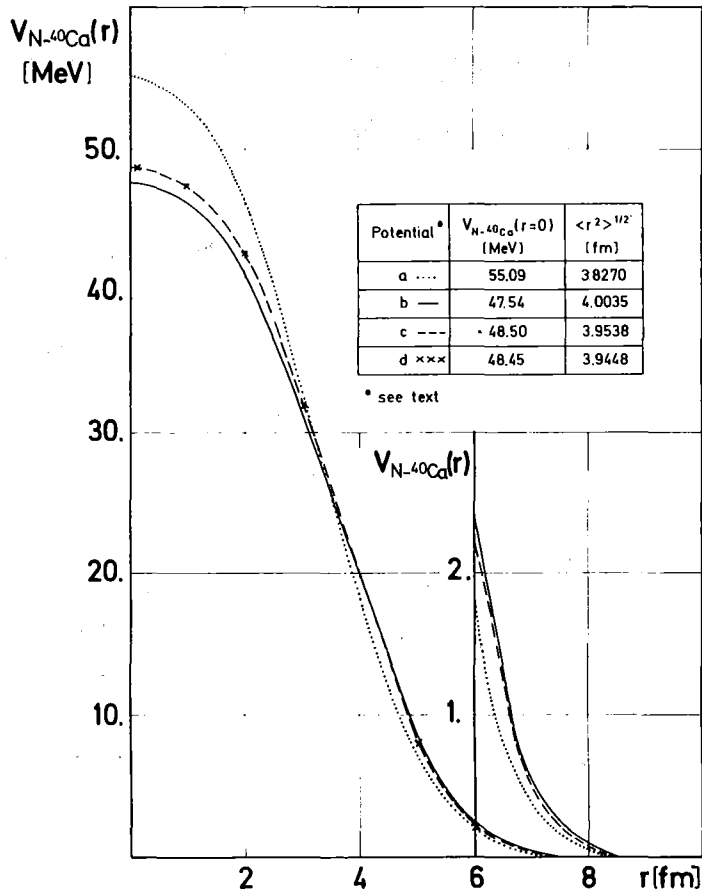 IM-intermediate approximation (m=0.5)

Fig. 12. Nucleon-^{40}Ca potentials microscopically calculated for different approximations of the density dependence of the NN interaction.

tion the normalization factor remains $\lambda_R < 1$.

Fig. 13 displays the experimental and theoretical differential cross sections corresponding to the results presented in tabs. 8 and 9.

5. FOLDED SPIN-ORBIT POTENTIAL FOR ELASTIC ^{6}Li-SCATTERING

The phenomenological analyses of elastic scattering of ^{6}Li from ^{40}Ca did not reveal very conclusive information on the presence of a spin-orbit term. In order to get some indication in which way such a term would affect the theoretical cross sections when included to the microscopically calculated potentials

Table 9   Optical model best fit parameters for $^{40}Ca(\alpha,\alpha)^{40}Ca$ and $^{40}Ca(^{6}Li,^{6}Li)^{40}Ca$ scattering. Corresponding theoretical differential cross sections are shown in fig. 13.

	Approach*	λ_R	m	W_V (MeV)	$D_2 \cdot A_T^{-1/3}$ (fm)	d_2 (fm)	W_s (MeV)	$D_3 \cdot A_T^{-1/3}$ (fm)	d_3 (fm)	χ^2/F
$^{40}Ca(\alpha,\alpha)$	SD	1.235	1.0	11.77	1.869	1.161	8.03	1.192	1.392	5.8
	IM	1.0	0.5	9.94	1.997	1.095	11.01	1.212	0.823	4.0
$^{40}Ca(^{6}Li,^{6}Li)$	SD	0.766	1.0	48.07	1.451	2.138	5.09	1.838	0.829	5.9

*SD - sudden approximation (m=1)

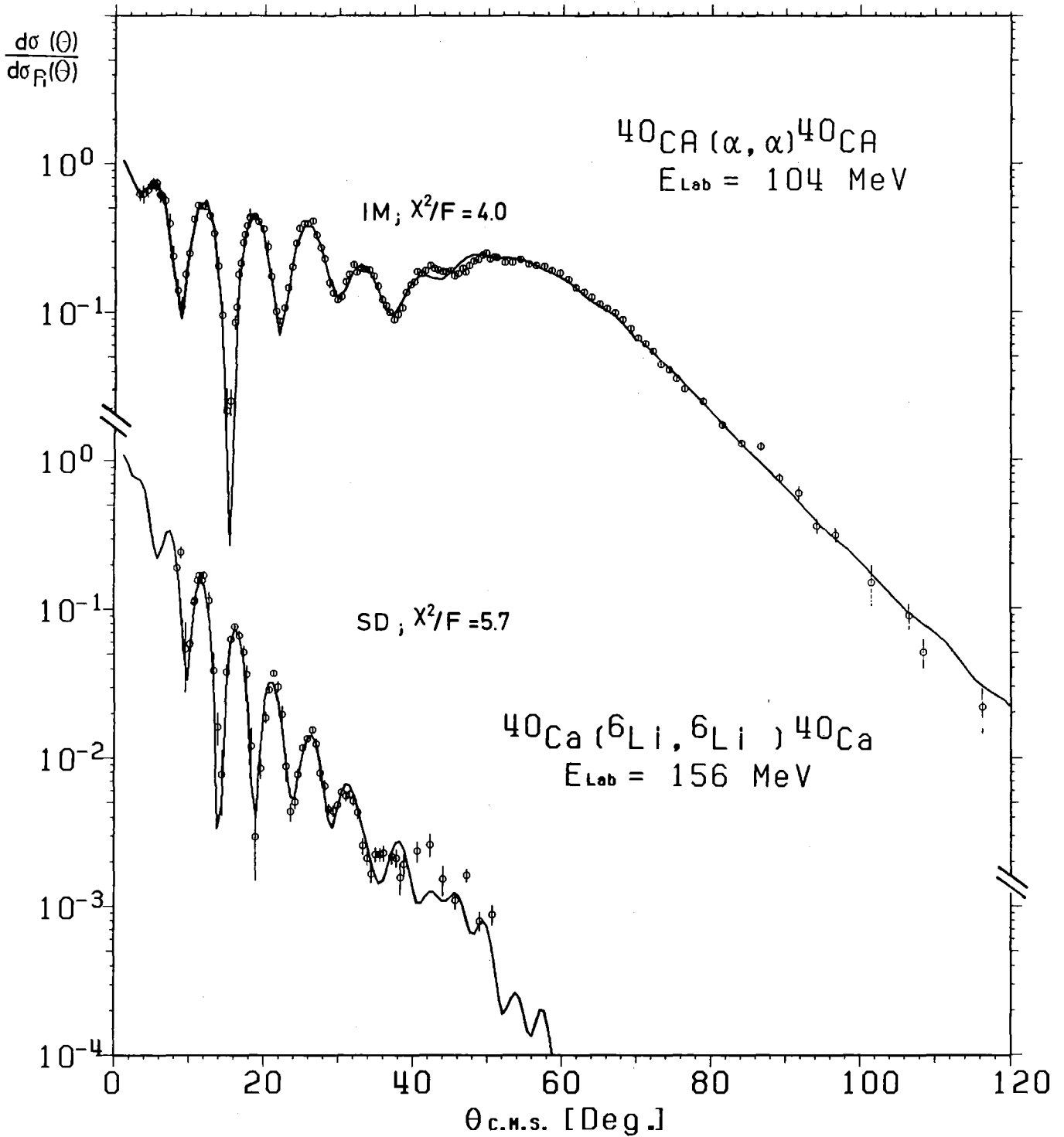 IM - intermediate approximation (m=0.5)

Fig. 13. Analyses of ^{40}Ca (α,α) ^{40}Ca at E_α = 104 MeV and ^{40}Ca(^{6}Li,^{6}Li)^{40}Ca at E_{Li} = 156 MeV on the basis of a double folding model with density dependent effective NN forces.

we generate the ^{6}Li-^{40}Ca spin-orbit interaction $V_{PT}^{LS}(r)$ by a folding procedure. Following Amakawa and K.I. Kubo /22/ the radial part of the spin-orbit potential is calculated in the form

$$V_{^6Li-40Ca}^{LS}(r) = \frac{2}{A_P}[\int d\vec{Z}_d \rho_d(\vec{Z}_\alpha)V_{ls}(\vec{x}) + \frac{(A_P-2)}{A_P r^2} \int d\vec{Z}_d(\vec{r}\cdot\vec{Z}_d)\rho_d(\vec{Z}_\alpha)V_{ls}(\vec{x})]$$

(5.1)

where $\vec{Z}_d$ represents the relative distance between the deuteron-cluster and the α-particle in the ^{6}Li projectile, $\vec{x}$ the distance between the deuteron cluster and the target nucleus. Using the derivative of Saxon-Woods form for the deuteron-target nucleus spin-orbit potential

$$V_{ls}(\vec{x}) = 2 \left(\frac{h}{m_\pi c}\right)^2 \frac{V_o}{x} \frac{d}{dx} f(x)$$

(5.2 a)

$$f(x) = \{1 + \exp((x-R_{LS})/a_{LS})\}^{-1}$$

(5.2 b)

with V_o=7 MeV, R_{LS}=1.25 $A_T^{1/3}$ fm and a_{LS}=0.75 fm, and introducing a Fermi form for ρ_d with $R_d = 1.2 A_T^{1/3}$ fm and $a_d = 0.65$ fm, the expression (5.1) has been evaluated. The parameters of the potential (5.2) are taken from experimental results of 52 MeV deuteron scattering /47/. Fig. 14 displays the resulting folded spin-orbit potential, which proves to be relatively weak in fair agreement with the phenomenological result (derivative form). For comparison the shape deduced as a derivative of the microscopically calculated central potential (normalized at r=5 fm) is shown in Fig. 16. The influence of the spin-orbit term on the differential cross sections is very small. The asymmetry $<i\ T_{11}>$ predicated for scattering of vector polarized ^{6}Li particles (P=1/$\sqrt{3}$) is shown in fig. 15. At this storage of the analyses we cannot finally test the importance of the spin-orbit potential for ^{6}Li ion scattering.
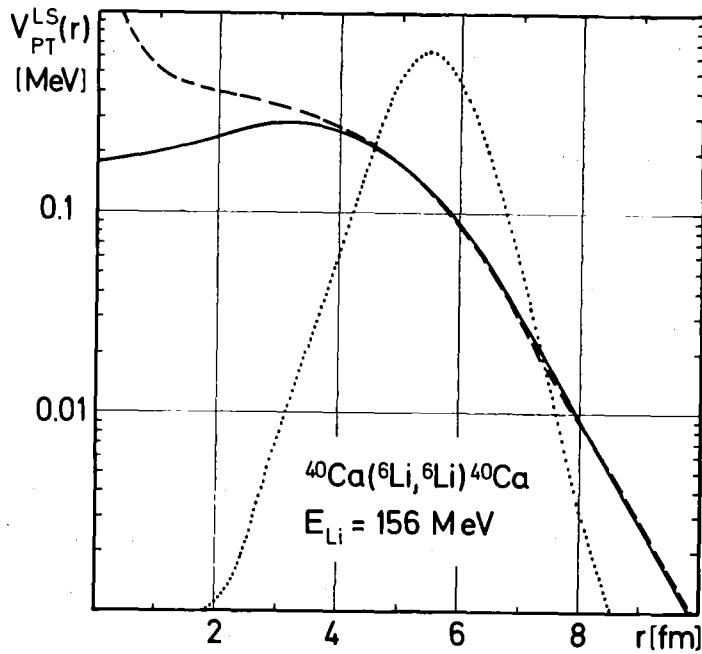
Fig. 14: ^{6}Li-^{40}Ca spin-orbit potentials: Folding procedure - solid line, derivative of the central real part of the folded potential normalized at r=5 fm - dashed line, phenomenological best fit - doted line.
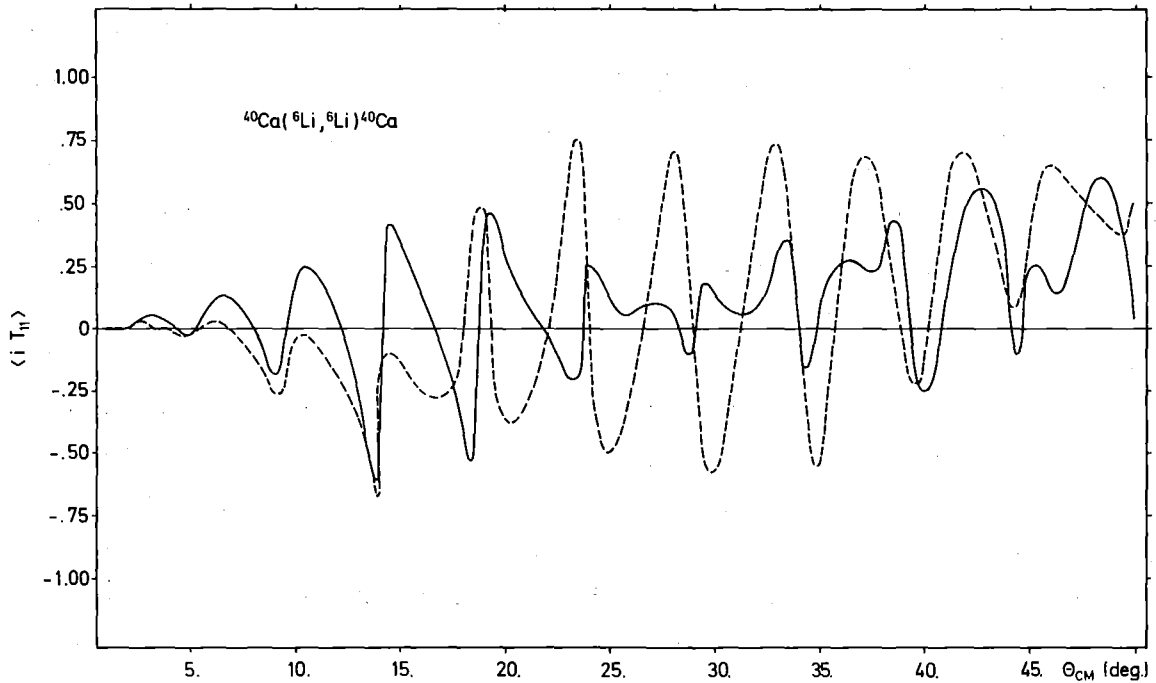

Fig. 15: Asymmetry $<iT_{11}>$ predicted for scattering of vector polarized ^{6}Li ions: folded spin-orbit potential - solid line, phenomenological best fit - dashed line.

6. SUMMARY AND CONCLUSIONS

In the present state a fully satisfactory theoretical treatement of all contributions to the real part of the microscopic composite particle-target nucleus potential is not in our reach. Our investigations are based on simple and refined double folding procedures in calculating the real part of the complex-projectile target nucleus potentials for 104 MeV alpha-particle and 156 MeV ^{6}Li elastic scattering from ^{40,48}Ca. The experimental background of our studies is characterized by accurate and precise determinations of the angular distributions which prove to be a necessary prerequisite of any reasonable conclusions on finer effects from comparison of theory and experiment.

In sect. 2 we obtained excellent fits to the experimental data using a modified phenomenological form of the optical potential. In contrast to the alpha-particle scattering where unambiguous potentials could be determined, for ^{6}Li-^{40}Ca scattering several equivalent potentials have been found. In agreement with a simple estimation (eq. 2.3) the microscopic calculations favour the family with $U_R(r=0) \simeq 180$ MeV.

Concerning the aspect of nuclear size purely phenomenological analysis only provides information on the optical potentials. However, one may assume that the difference between the mean-square (ms) radii of the potentials for α-^{48}Ca and α-^{40}Ca scattering is equal to the difference between the ms radii of the nuclear matter density distributions. From table 1 we obtain $<r^2>_v$ (^{48}Ca) $- <r^2>_v$ (^{40}Ca) = 0.91 fm^2, and adopting the value /38/ $<r>_m^{1/2}(^{40}$Ca) = 3.37 fm we find $<r^2>_m^{1/2}(^{48}$Ca) $- <r>_m^{1/2}(^{40}$Ca) = 0.13 fm in agreement with other studies /23/.

Following the theoretical procedures described in the first part of sect. 3 we studied and detect the validity of the real part of the simple direct projectile and target folding potentials for alpha-particle and ^{6}Li ions scattering. The procedures include the one-nucleon exchange and the density dependence of the nucleon-nucleon interaction in the nucleon-nucleus system. The main results of these studies may be summarized by following statements:

a) Experimental 104 MeV α-particle and 156 MeV ^{6}Li-ion scattering cross sections can satisfactoryly be described up to large scattering angles by folding models only if one includes density dependence and exchange effects of the NN-interaction in the nucleon-target system. The quality of the fits obtained is nearly the same as by use of phenomenological optical potentials.

b) One nucleon exchange effects are of minor importance as compared to density dependence of the nucleon-nucleon interaction.

Since for the procedures used in sect. 3 normalization factors of the real potential < 1 proved to be necessary, in sect. 4 we additionally refined the folding procedures by taking into account the dependence of the nucleon-nucleon interaction on the density of *both* colliding nuclei. These investigations yielded the two following results.

c) Fully satisfactory description of elastic α-particle scattering cross sections including large angle data is obtained *without any futher renormalization* of the real part of the potential.

d) For ^{6}Li-scattering good representation of the experimental data can only be obtained by requiring a normalization factor of the microscopic optical potential smaller than 1.

The general difference between the results for α-particle and ^{6}Li-scattering [c) and d)] may partly be due to the fact, that the α-particle is strongly bound in contrast to the ^{6}Li-ion, where the coupling of the dominant break-up channel may influence the elastic scattering channel significantly. In fact, this result supports the conclusions /41/ that ^{6}Li behaves in a way somewhat different than the lighter projectiles.

In order to remove some uncertainty resulting from the chosen nucleon-nucleon interaction we applied the "new realistic" nucleon-nucleon interaction /40,48/ which reproduces within the framework of the folding model ion-ion potentials for ^{12}C and ^{16}O scattering satisfactorily /40,49/. As already presented in ref. /50/, this interaction fails in our cases.

Looking, once more, to the question of extracting nuclear size information by folding model analyses of elastic α-scattering, we like to conclude as follows:

e) The uncertainties of treating the effective interaction in early
   folding models have been removed to an important part, so that
   now influences of the nuclear matter densities chosen clearly
   come up. In fact, introducing the neutron density distribution
   $\rho_n \neq N/Z \; \rho_p$ for ^{48}Ca significantly better fits to the experi-
   mental data have been obtained.

This is a decisive argument to use the folding approach in this
way to extract nuclear size information particularly neutron
density radii from elastic α-particle scattering cross sections.
Finally, some preliminary calculations where phenomenological
and semi-mircoscopic spin-orbit potentials were included indicate
that for 156 MeV ^{6}Li ion scattering spin-orbit effects are very
small.

   Concluding, we would like to underline that folded potentials
with density dependence effects included are appropriate for
description of light complex ion scattering.

REFERENCES

/1/ H.H. Chang, B.W. Ridley, T.H. Braid, T.W. Conlon,
     E.F. Gibson and N.S.P. King, Nucl. Phys. A270 (1976) 419.

/2/ L.W. Put and A.M. Paans, Nucl. Phys. A 291 (1977) 93.

/3/ N.S. Wall, A.A. Cowley, R.C. Johnson and A.M. Kobos,
     Tech. Report No. 77-046, University of Maryland,
     Dept. Physics (Jan. 1977).

/4/ D.F. Jackson and V.K. Kembhavi, Phys. Rev. 178 (1969) 1626.

/5/ P.P. Singh, P. Schwandt and G.C. Yang, Phys. Lett. 59 B,
     (1975) 113.

/6/ A. Budzanowski, A. Dudek, K. Grotowski and A. Strzałkowski,
     Phys. Lett. 32 B (1970) 431;
     A. Budzanowski, A. Dudek, K. Grotowski,Z. Majka and
     A. Strzałkowski, Particle and Nuclei 5 (1973)97.

/7/ Z. Majka, A. Budzanowski, K. Grotowski, A. Strzałkowski,
     Phys. Rev. C, in press, - Proc. EPS Conference on Radial
     Shape of Nuclei, Cracow (1976) 135.

/8/ J.P. Vary and C.B. Dover, Phys. Rev. Lett. 31 (1973) 1510.

/9/ G.R. Satchler, Phys. Lett. 59B (1975) 121.

/10/ R. Schaeffer, Nucl. Phys. A 158 (1970) 321.

/11/ A. Budzanowski, H. Dabrowski, L. Freindl, K. Grotowski,
      S. Micek, R. Płaneta, A. Strzałkowski, M. Bosman,
      P. Leceux, P. Macq, J.-P. Meulders, C. Pieraut, Phys.
      Rev. 17 C (1978)951; Z.Majka, T. Srokowski, Acta Phys.
      Polonica B9 (1978) 53.

/12/ B. Sinha, Phys. Lett. 33 (1974).

/13/ I. Brissaud and M.K. Brussel, Phys. Rev. C13 (1976) 1748.

/14/ F. Petrovich, D. Stanley and J.J. Bevelacqua, Phys.
      Lett. 71 B (1977) 259.

/15/ W.G. Love, Phys. Lett. 72B (1977) 4.

/16/ Y. Eisen and B. Day, Phys. Lett. 63B (1976) 1976.

/17/ H. Rebel, Proc. EPS Conf. on Radial Shape of Nuclei,
      Cracow (1976) and references quoted therein.

/18/ G. Hauser, R. Löhken, H. Rebel, G. Schatz, G.W. Schweimer,
      J. Specht, Nucl. Phys. A 128 (1968) 563.

/19/ D.A. Goldberg and S.M. Smith, Phys. Rev. Lett. 29
     (1972) 500.

/20/ D.A. Goldberg, Invited Talk at the Sympos. on Heavy Ion
     Scattering, Rochester, Oct. 25-26, 1977, Techn. Rep.
     78-050/University of Maryland, Dept. of Physics, Oct. 1977.

/21/ J.G. Cramer, R.M. DeVries, D.A. Goldberg, M.S. Zisman
     and C.F. Maguire, Phys. Rev. C14 (1976) 2158.

/22/ A. Amakawa and K.I. Kubo, Nucl. Phys. A 266 (1976) 521;
     W. Weiss, P. Egelhof, K.D. Hildenbrand, D. Kassen,
     M. Makowska-Rzeszutko, D. Fick, H. Ebinghaus, E. Steffens,
     A. Amakawa and K.I. Kubo, Phys. Lett. 61B (1976) 237.

/23/ H.J. Gils, H. Rebel, E. Friedman, Z. Majka, Proc. XVI Int.
     Winter Meeting on Nucl. Phys., Bormio (Italy) Jan.16-20,1978;
     E. Friedman, H.J. Gils, H. Rebel, Z. Majka, to be
     published.

/24/ J. Buschmann, H.J. Gils, H. Rebel, Z. Majka and
     S. Zagromski, to be published.

/25/ J. Buschmann, H.J. Gils, H. Rebel, S. Zagromski,
     G. Bechtold, H. Klewe-Nebenius, H, Faust and B. Neumann,
     Verhandlg. DPG 4/1978, S. 945.

/26/ H.M. Hussein and O. Zohni, Nucl. Phys. A 267 (1976) 303.

/27/ J.S. Lilley, Phys. Rev. C3 (1971) 2229.
     P. Mailandt, J.S. Lilley and G.W. Greenlees, Phys. Rev.
     C8 (1973) 2189.

/28/ A.M. Bernstein, Advances in Nucl. Phys., ed. by M. Baranger
     and E.Vogt (Plenum Press, New York 1969).

/29/ B. Tatischeff, I. Brissaud and L. Bimbot, Phys. Rev. C5
     (1972) 234.

/30/ H. Rebel, R. Löhken, G.W. Schweimer, G. Schatz and G. Hauser,
     Z. Physik 256 (1972) 258.

/31/ J. Brissaud, Y. Le Bornec, B. Tatischeff, L. Bimbot,
     M.K. Brussel and G. Duhamel, Nucl. Phys. A 191 (1972) 145.

/32/ D.F. Jackson and R.C. Johnson, Phys. Lett. 49B (1974) 249.

/33/ J.C. Slater, Phys. Rev. 81 (1931) 385.

/34/ V.R. Pandharipande, Nucl. Phys. A166 (1971) 317.

/35/ A. Kallio and K. Kolltveit, Nucl. Phys. 33 (1964) 8.

/36/ A.M. Green, Phys. Lett. 24B (1967) 384.

/37/ M.M. Block, I. Kenyon, J. Keren, D. Koetke, P. Malhotra,
     P. Mazur, R. Walker and H. Winzeler, Phys. Lett. 26B
     (1968) 464.

/38/ W. Bertozzi, J. Friar, J. Heisenberg and J.W. Negele,
     Phys. Lett. 41B (1972) 408.

/39/ H.D. Wohlfahrt, E.B. Shera, M.V. Hochn, Y. Yamazaki,
     G. Fricke and R.M. Steffen, Phys. Lett. 73B (1978) 131.

/40/ G.R. Satchler and W.G . Love, Phys. Lett. 65B (1976) 415.

/41/ G.R. Satchler and W.G. Love, Preprint 1978 - G.R. Satchler
     private communications.

/42/ Z. Majka, Phys. Lett., in press.

/43/ G.C. Li, I. Sick. R.R. Whitney and M.R. Yearian,
     Nucl. Phys. A162 (1971) 583.

/44/ W.G. Love, Phys. Lett. 72B (1977) 4.

/45/ E. Friedman and C.J. Batty, Phys. Rev. C17 (1978) 34.

/46/ W.P. Myers, Nucl. Phys. A 204 (1973) 465.

/47/ F. Hinterberger, G. Mairle, U. Schmidt-Rohr, G.J. Wagner
     and P. Turek, Nucl. Phys. A 111 (1968) 265.

/48/ G. Bertsch, J. Borysowicz, H. McManus, W.G. Love,
     Nucl. Phys. A 284 (1977) 399.

/49/ G.R. Satchler, Nucl. Phys. A 279 (1977), R.M. Wieland,
     R.G. Stokstad, G.R. Satchler, L.D. Rickertson, Phys. Rev.
     Lett. 37 (1976) 1458.

/50/ Z. Majka, H. Rebel, H.J. Gils, 3rd International Conference
     on Clustering Aspects of Nuclear Structure and Nuclear
     Reaction, Manitoba (June 19-23, 1978).

/51/ R.F. Frosch, R. Hofstadter, J.S. McCarthy, G.K. Noldeke,
     K.J. van Oostrum, B.C. Clark, R. Herman, D.G. Rawenhall,
     Phys. Rev. 174 (1978) 1380.

Appendix:
Experimental cross sections of 156 MeV ^{6}Li on ^{40}Ca

SCATTERING OF 6-LI PARTICLES ON 4C-CA

ELAB = 156.000 MEV   Q = 0.0   MEV   I = 0 +

ECM = 135.591 MEV   K = 5.8242/FERMI   ETA = 1.85545

| LABORATORY DATA | | | RUTHERFORD | CM DATA | | |
THETA DEGREE	SIGMA MB/SR	DSIGMA %	SIGMA/SR	THETA DEGREE	SIGMA MB/SR	DSIGMA MB/SR
7.25	2.276E+03	1.1	1.910E-01	8.36	1.713E+03	1.835E+01
7.75	2.219E+03	8.6	2.430E-01	8.94	1.670E+03	1.431E+02
8.25	3.865E+02	48.8	5.433E-02	9.52	2.910E+02	1.422E+02
8.75	3.318E+02	6.9	5.9C0E-02	10.09	2.499C+02	1.737E+01
9.25	5.038E+02	4.6	1.118E-01	10.67	3.796E+02	1.741E+01
9.39	4.385E+02	3.5	1.151E-01	10.83	3.682E+02	1.295E+01
9.75	5.720E+02	3.2	1.566E-01	11.25	4.312E+02	1.388E+01
9.89	5.985E+02	3.8	1.7C6E-01	11.41	4.437E+02	1.705E+01
10.25	4.704E+02	4.3	1.572E-01	11.82	3.547E+02	1.527C+01
1C.39	4.794E+02	4.5	1.692E-01	11.98	3.616E+02	1.616E+01
11.00	2.585E+02	14.2	1.145E-01	12.69	1.951E+02	2.763E+01
11.50	7.385E+01	31.6	3.9C6E-02	13.26	5.576E+01	1.761E+01
12.00	2.573E+01	24.7	1.613E-02	13.84	1.944E+01	4.799E+00
12.50	1.048E+01	46.6	7.731E-03	14.41	7.924E+00	3.691E+00
13.00	4.393E+01	12.2	3.788E-02	14.99	3.323E+01	4.061C+00
13.50	6.311E+01	3.7	6.324E-02	15.56	4.776E+01	1.749E+00
14.00	6.599E+01	3.0	7.642E-02	16.14	4.996E+01	1.519E+C0
14.50	5.036E+01	6.7	6.7C6E-02	16.71	3.815E+01	2.552E+00
15.00	3.400E+01	9.5	5.182E-02	17.29	2.578E+01	2.458E+00
15.39	2.174E+01	14.4	3.670E-02	17.73	1.649E+01	2.371E+00
15.89	6.271E+00	32.5	1.2C2E-02	18.31	4.759E+00	1.549E+00
16.39	1.353E+00	49.2	2.932E-03	18.88	1.028E+00	5.054E-01
17.00	3.391E+00	14.7	8.497E-03	19.58	2.578E+00	3.798E-01
17.50	6.652E+00	3.7	1.870E-02	20.16	5.06CE+00	4.412E-01
18.00	9.139E+00	5.1	2.873E-02	20.73	6.958E+00	3.565E-01
18.50	1.063E+01	4.3	3.725E-02	21.30	8.097E+00	3.482E-01
19.00	7.787E+00	7.8	3.034E-02	21.88	5.938E+00	4.652E-01
19.50	4.589E+00	13.5	1.982E-02	22.45	3.502E+00	4.727C-01
20.00	1.840E+00	20.7	8.786E-03	23.02	1.406E+00	2.9C8E-01
20.50	8.241E-01	13.4	4.338E-03	23.59	6.300E-01	8.418E-02
21.00	8.761E-01	10.5	5.C73E-03	24.17	6.704E-01	7.012E-02
21.39	1.251E+00	8.1	7.792E-03	24.61	9.58CE-01	7.736E-02
21.89	1.727E+00	3.7	1.178E-02	25.18	1.323E+00	4.953E-02
22.39	1.811E+00	3.7	1.351E-02	25.76	1.389E+00	5.094E-02
23.00	1.357E+00	3.4	1.540E-02	26.45	1.426E+00	4.877E-02
23.50	1.385E+00	7.8	1.250E-02	27.02	1.065E+00	8.319E-02
24.00	8.105E-01	10.8	7.952E-03	27.59	6.238E-01	6.740E-02
24.50	6.161E-01	7.7	6.556E-03	28.16	4.747E-01	3.657E-02
25.00	3.936E-01	7.7	4.535E-C3	28.73	3.036C-01	2.326E-02
25.50	3.553E-01	8.0	4.426E-03	29.30	2.743E-01	2.187E-02
26.00	3.594E-01	4.7	4.832E-03	29.87	2.778E-01	1.319E-02
26.50	4.078E-01	4.3	5.9C9E-03	3C.44	3.155E-01	1.363E-02
27.00	3.553E-01	7.8	5.540E-03	31.01	2.752E-01	2.159E-02
27.39	3.45CE-01	5.8	5.692E-03	31.45	2.675E-01	1.553E-02
27.89	2.891E-01	6.7	5.120E-03	32.02	2.244C-01	1.497E-02
28.39	2.266E-01	9.3	4.303E-03	32.59	1.761E-01	1.643L-02
29.00	1.245E-01	12.6	2.569E-03	33.28	9.688E-02	1.217E-02
29.50	9.587E-02	10.4	2.115E-03	33.85	7.471E-02	7.798E-03
30.00	7.073E-02	13.1	1.667E-03	34.42	5.519E-02	7.254E-03
30.50	8.897E-02	11.2	2.236E-03	34.98	6.951E-02	7.763C-03
31.00	8.353E-02	10.0	2.236E-03	35.55	6.532E-02	6.506E-03
31.50	8.002E-02	11.5	2.281E-03	36.12	6.269E-02	7.234E-03
32.50	6.680E-02	10.5	2.151E-03	37.25	5.247E-02	5.515E-03
33.00	6.190E-02	12.9	2.115E-03	37.81	4.868E-02	6.271E-03
33.45	4.358E-02	23.5	1.570E-03	38.32	3.432E-02	8.069E-03
33.89	5.062E-02	16.5	1.918E-03	38.82	3.991E-02	6.595E-03
35.50	5.205E-02	15.6	2.362E-03	40.63	4.124E-02	6.441E-03
37.00	4.895E-02	17.0	2.606E-03	42.32	3.895E-02	6.624E-03
38.50	2.454E-02	22.8	1.523E-03	44.00	1.962E-02	4.479E-03
40.00	1.519E-02	12.4	1.092E-03	45.68	1.220E-02	1.518E-03
41.39	1.977E-02	9.9	1.620E-03	47.23	1.596E-02	1.584E-03
43.00	8.416E-03	14.8	7.979E-04	49.03	6.831E-03	1.0C9E-03
44.50	8.159E-03	15.1	8.813E-04	50.70	6.657E-03	1.004E-03

9 June 1978